Structure of a human monoclonal antibody in complex with Outer surface protein C (OspC) of the Lyme disease spirochete, *Borreliella burgdorferi*

Michael J. Rudolph[1,*], Yang Chen[1], Clint Vorauer[2], David J Vance[3,4], Carol Lyn Piazza[3], Graham G Willsey[3], Kathleen McCarthy[4] Beatrice Muriuki[5], Lisa A. Cavacini[5], Miklos Guttman[2], and Nicholas J Mantis[3,4,*]

[1]New York Structural Biology Center, New York, NY; [2]Department of Medicinal Chemistry, University of Washington, Seattle, WA; [3]Division of Infectious Diseases, Wadsworth Center, New York State Department of Health, Albany, NY; Department of Biomedical Sciences, University at Albany, Albany, NY; [5]University of Massachusetts Chan Medical School, Worcester, MA

To whom correspondence should be addressed:
Michael J Rudolph, mrudolph@nysbc.org
Nicholas J. Mantis, nicholas.mantis@health.ny.gov

Running title: Human antibody in complex with OspC

Keywords: antibody, human, epitope, infection, vaccine

Abstract

Lyme disease is a tick-borne, multisystem infection caused by the spirochete, *Borreliella burgdorferi*. Although antibodies have been implicated in the resolution of Lyme disease, the specific B cell epitopes targeted during human infections remain largely unknown. In this study, we characterized and defined the structural epitope of a patient-derived bactericidal monoclonal IgG ("B11") against Outer surface protein C (OspC), a homodimeric lipoprotein necessary for *B. burgdorferi* tick-mediated transmission and early-stage colonization of vertebrate hosts. High-resolution epitope mapping was accomplished through hydrogen deuterium exchange-mass spectrometry (HDX-MS) and X-ray crystallography. Structural analysis of B11 Fab-$OspC_A$ complexes revealed the B11 Fabs associated in a 1:1 stoichiometry with the lateral faces of $OspC_A$ homodimers such that the antibodies are essentially positioned perpendicular to the spirochete's outer surface. B11's primary contacts reside within the membrane proximal regions of α-helices 1 and 6 and adjacent loops 5 and 6 in one $OspC_A$ monomer. In addition, B11 spans the $OspC_A$ dimer interface, engaging opposing α-helix 1', α-helix 2', and loop 2-3' in the second $OspC_A$ monomer. The B11-$OspC_A$ structure is reminiscent of the recently solved mouse transmission blocking monoclonal IgG B5 in complex with $OspC_A$, indicating a mode of engagement with OspC that is conserved across species. In conclusion, we provide the first detailed insight into the interaction between a functional human antibody and an immunodominant Lyme disease antigen long considered an important vaccine target.

Introduction

Lyme borreliosis or Lyme disease is the most common vector-borne infection in the United States, with an estimated 450,000 cases per year [1]. The primary etiologic agent of Lyme disease is the spirochete bacterium, *Borreliella burgdorferi* sensu latu (herein referred to as simply *B. burgdorferi*). In North America, the spirochete is transmitted to humans by black legged ticks, *Ixodes scapularis* and *Ixodes pacificus*, during the course of a blood meal. The spirochete proliferates at the site of the tick bite, typically resulting in an expanding skin lesion commonly referred to as a bull's eye rash or erythema migrans [2-4]. In the absence of antibiotic intervention, *B. burgdorferi* disseminates to peripheral tissues, organs, large joints, and the central nervous system, potentially resulting in severe complications including neuroborreliosis, carditis and/or Lyme arthritis [2, 5]. A fraction of Lyme disease patients who receive a full regimen of antibiotics will report persistent health issues (e.g., fatigue, cognitive issues, musculoskeletal pain), a syndrome referred to as post-treatment Lyme disease (PTLD) [6-8].

In an effort to define the immunologic factors that drive resolution of Lyme disease, Blum and colleagues characterized B cell responses in patients across the course of infection [9]. Blood plasmablasts from Lyme disease patients and a healthy cohort were subjected to bulk BCR and single cell paired V_H and V_L sequencing [9]. The analysis revealed that robust plasmablast responses correlated with a more rapid resolution of disease symptoms. Moreover, expression of a panel of recombinant human monoclonal antibodies (MAbs) using paired V_H and V_L sequences from representative clones were screened for reactivity with *B. burgdorferi* antigens. The "hits" included a number of immunodominant *B. burgdorferi* surface lipoproteins previously known to be reactive in convalescent human Lyme disease sera, including VlsE, DbpA, DbpB and OspC [9-11]. The recombinant MAbs were further screened for the ability to inhibit growth of *B. burgdorferi* strain B31 in culture. Of the six MAbs with borreliastatic activity (and therefore implicated in disease resolution), two (B2 and B11) were directed against OspC.

Outer surface protein C (OspC) is a member of the small variable surface protein (Vsp) family of immunodominant antigens unique to *Borrelia* and *Borreliella* including the relapsing fever spirochetes (*B. turicatae*) [12]. In *B. burgdorferi*, OspC is expressed during tick transmission and in the early stages of mammalian infection [13-15]. During this period, OspC plays a multifaceted role in pathogenesis, including facilitating spirochete egress from the tick during the course of a blood meal, enabling survival in the early stages of mammalian skin

infection, plasminogen interactions, and modulating transmigration across vascular walls [14-20]. The importance of OspC in *B. burgdorferi* pathogenesis is underscored by the fact that active vaccination with recombinant OspC or passive transfer of OspC antibodies completely prevent tick-mediated *B. burgdorferi* infections in mouse models [21-25]. However, while only a single copy of *ospC* is encoded on any *B. burgdorferi* genome, there are >26 *ospC* types and subtypes within *B. burgdorferi* isolates in North America, with multiple types often found in the same geographical proximity [26-28]. The polymorphic nature of OspC is proposed to constitute a means of *B. burgdorferi* immune evasion, as antibodies to one OspC type have limited cross-reactivity and cross-protection with other OspC types [28-31].

Structurally, OspC is ~21 kDa helical bundle that forms homodimers on the spirochete outer surface [32-36]. Despite a high degree of amino acid variability across the different OspC types, the tertiary and quaternary structures of OspC are virtually identical. As OspC's N-termini are anchored in the outer membrane via a lipid moiety, the molecule is generally depicted with the stem tethered to the spirochete surface and the dome, with more variable residues, projecting outward [35]. As such it is reasonable to expect that type-specific antibodies target the outward face of OspC, occluding the putative ligand binding cavities [35]. However, the X-ray crystal structure of OspC type A ($OspC_A$) complexed with the mouse MAb, B5, reveals a more complicated picture. B5 is the most well-characterized OspC monoclonal antibody originally isolated from *B. burgdorferi*-infected mice [23, 37]. In passive immunization studies, B5 blocks tick-mediated transmission of *B. burgdorferi*, presumably by entrapping the spirochetes in the tick midgut [23]. The X-ray crystal structure revealed that B5 Fabs associates at a nearly perpendicular angle with the lateral sides of homodimeric $OspC_A$ [38]. The side-on orientation of B5 with $OspC_A$ raises questions about the mechanisms by which the antibody interferes with spirochetal transmission as the putative ligand binding pockets on the outer most face of OspC are unobstructed. A limited insight into the nature of OspC-antibody interactions in mice (and none in humans) represents a gap in our understanding of a critical immune interaction with implications for both Lyme disease resolution and vaccine design. In this study, we report the structure of the human MAb B11 in complex with OspC and its impact on *B. burgdorferi* viability *in vitro*.

Results

MAb B11 recognition of native and recombinant OspC

The human MAb, B11, was originally isolated by Blum and colleagues as a recombinant IgG1 with paired V_H and V_L sequences from single-cell sorted, blood-derived plasmablasts from a Lyme disease patient [9]. The B11 V_H and V_L sequences are assigned germline HV4-39 and KV3-15, based on the IMGT database[39]. Based on that assignment, the B11 V_H and V_L coding regions have as many as 16 amino acid mutations from V_H HV4-39 germline and 10 from the V_L KV3-15 germline, suggesting the antibody has undergone significant somatic hypermutation. Analysis of the available BioProject database indicate that one other B11 clone exists, alongside three closely related clones all derived from the same patient (D. Vance, *unpublished observations*).

The B11 V_H and V_L coding regions were cloned in-frame into pcDNA3.1-based human IgG_1 Fc and kappa light chain expression plasmids, respectively, and then co-transfected into Expi293 cells. Purified B11 IgG1 was assessed for the ability to recognize native OspC. Live *B. burgdorferi* strains expressing $OspC_A$ (strain B313), $OspC_B$ (strain ZS7), or $OspC_K$ (strain 297) were incubated with B11 IgG_1 or an isotype control (PB10 IgG_1), then subjected to flow cytometry (**Figure 1**). A B31 derivative lacking *ospC* (B31A Δ*ospC*) was also included as a control [40]. By flow cytometry, B11 was highly reactive with strain B313 expressing $OspC_A$ (MFI >3300), but not with the *B. burgdorferi* Δ*ospC* mutant. Moreover, MAb B11 did not react with strain ZS7 expressing $OspC_B$ (MFI <35) or 297 expressing $OspC_K$ (MFI <35), indicating that B11 recognition of OspC is type restricted. Indeed, we employed BLI to examine B11 reactivity with recombinant dimeric $OspC_A$. In that assay, B11 IgG had an apparent dissociation constant (K_D) of ~39 nM for recombinant dimeric $OspC_A$ (**Figure S1**), but negligible reactivity with $OspC_B$ or $OspC_K$ (**data not shown**). This OspC reactivity profile is reminiscent of MAb B5 [38].

MAb B11 promotes *B. burgdorferi* agglutination and alterations in outer membrane permeability.

We recently reported that antibody-mediated agglutination of live *B. burgdorferi* spirochetes results in flow cytometric events with increased size (FSC) and granularity (SSC) [41]. Furthermore, the addition of propidium iodide (PI) to the spirochete preparations just prior to flow cytometry serves as indicator of antibody-induced changes to OM permeability [41]. We

have postulated that antibody-mediated agglutination explains, at least in part, how OspA and possibly OspC antibodies compromise *B. burgdorferi* within the tick midgut and limit their transmission to vertebrate hosts [23, 30, 38]. We therefore examined what impact that B11 had on *B. burgdorferi* agglutination. Following B11 treatment, we observed significant *B. burgdorferi* B313 agglutination (20-25% of the population) with a fraction of aggregated cells also PI^+. This level of agglutination and PI^+ staining is similar to what we have observed previously for MAb B5 (**Figure 1B**). Neither MAb B11 nor B5 influenced agglutination or PI positivity of the *B. burgdorferi* Δ*ospC* mutant or *B. burgdorferi* strains ZS7 or 297 (**Figure 1B; data not shown**). Thus, B11 recognizes $OspC_A$ on the spirochete surface and has the propensity to promote both spirochete agglutination and alterations in outer membrane permeability in the absence of human complement.

Complement-dependent and independent impact of MAb B11 on *B. burgdorferi* motility

Blum and colleagues reported that MAb B11 (20 μg/mL) had growth inhibitory (bacteriostatic) activity on *B. burgdorferi* in standard culture conditions (BSK II) [9]. To confirm this observation, we examined *B. burgdorferi* B31 motility (as a proxy for cell viability) in the absence and presence of 20% human complement across a range of B11 doses (1-30 μg/mL). To circumvent issues associated with intrinsically low OspC expression by *B. burgdorferi* B31 in culture, we utilized a strain with an IPTG inducible *rpoS* allele, thereby activating native *ospC* expression in *trans* (see Methods). In the absence of complement, B11 had a modest effect on bacterial motility that but did not reach statistical significance as compared to an the isotype control, PB10 (**Figure 2**). The addition of human complement resulted in significant reduction in bacterial motility at B11 concentrations at 3 μg/ml and above. The transmission blocking MAb B5 was significantly more potent than B11 at arresting *B. burgdorferi* motility in absence of human complement and was similar to B11 in the presence of complement (**Figure 2**). Thus, in our hands, B11's effects on spirochete motility arrest are complement-dependent.

Localization of MAb B11's epitope on $OspC_A$ by HX-MS.

We employed HX-MS as a means of identifying B11's epitope on $OspC_A$. A series of preliminary quench and digestion experiments revealed that proteolysis of recombinant dimeric $OspC_A$ with Nepenthesin II (without the addition of urea) generated the largest set of observable

peptides. Filtering out weak and overlapping signals resulted in 74 unique peptides with a sequence coverage of 98.8% and redundancy of 5.3. The addition of MAb B11 IgG resulted in strong protection at residues 49-57 and 186-196, corresponding to the N- and C-termini of $OspC_A$, respectively (**Figure 3; Supplemental Excel file**). Moderate protection was also observed elsewhere (e.g., peptide 157-162). The B11 IgG HX-MS protection profile is reminiscent of the profile we reported for B5 IgG using slightly different HX-MS conditions [38]. To enable a direct comparison between B11 and B5, we subjected $OspC_A$ to HX-MS with B5 IgG under the same conditions as B11. The results revealed that HX-MS profiles were indeed distinct with B5 causing notably stronger protection at residues 72-80, 157-176, and 186-196, further from the N/C termini (**Figure 3**). These results suggest that B5 and B11 recognize overlapping but distinct epitopes primarily focused on $OspC_A$'s α-helix 5 and 6. To test this experimentally, we performed competitive binding assays between B5 and B11 using the BLI platform in which $OspC_A$ was first saturated with B5 then probed with B11. The results confirmed that B11's ability to associate with $OspC_A$ is abrogated by B5 occupancy (**Figure S1C**).

Structural analysis of the Fab B11-$OspC_A$ complex.

To resolve B11's epitope on $OspC_A$ in greater detail, we solved the X-ray crystal structure of B11 Fabs in complex with $OspC_A$ at 3.1 Å resolution in the P1 space group. The structure revealed two B11 Fabs bound to a single $OspC_A$ homodimer (1:1 Fab:$OspC_A$ stoichiometry) in a side-on fashion reminiscent (at first glance) of the B5 Fab-$OspC_A$ complex (**Figure 4**) . The B11 Fab fragments (Fab, Fab') made identical contacts on opposite sides of the $OspC_A$ homodimer ($OspC_A$-$OspC_A$'), as described in detail below. Each B11 Fab assumed the canonical antibody structure with two heavy chain immunoglobulin domains (V_H, C_H1) and two light immunoglobulin domains (V_L, C_L) each containing 7-10 β-strands arranged in two β-sheets that fold into a two-layer β-sandwich. The six CDRs (LCDR1-3, HCDR1-3) were situated on one face of the molecule. The four B11 FAb-$OspC_A$ complexes within the asymmetric unit were structurally similar, with Root-Mean-Square Deviations (RMSD) in the range of 0.8-1.8 Å upon Cα-superpositioning. $OspC_A$ homodimers in the absence and presence of B11 Fabs were also structurally nearly identical [RMSD of 0.6 Å], demonstrating that the B11 Fabs do not induce any significant conformational changes $OspC_A$.

Each B11 Fab contacted α-helix 1, α-helix 6, loop 5 (located between α-helices 5 and 6) and loop 6 (after α-helix 6) of their respective $OspC_A$ monomers. In addition, the Fabs each bridged the $OspC_A$ dimer interface with residues from HCDR1, HCRD3, and LCDR2 engageing with α-helix 1', α-helix 2', and loop 2' on the opposing $OspC_A$ molecule (**Figure 5A, B**), thereby demonstrating that B11's epitope is quaternary in nature. The B11 Fab and $OspC_A$ interface buried a total surface area ranging from 2,406 $Å^2$ to 2,772 $Å^2$ (**Table 2**) Shape complementarity (SC) scores ranged between 0.44-0.59 within the eight Fab-$OspC_A$ interfaces in the asymmetric unit, while H-bonds ranged from 3 to 13 and salt bridges from 2 to 4.

While all six B11 CDR elements (L1-L3 and H1-H3) associated with $OspC_A$, the bulk of the interaction was mediated by HCDR1-3. Specifically, the B11 V_H domain accounted for ~75% of the total BSA within the complex and most of the H-bonds and salt bridges. Key H-bonds include HCDR1 Ser-33 with $OspC_A$ Lys-60, and HCDR2 residue Tyr-54 with $OspC_A$ Glu-63, with a notable salt bridge occurring between HCDR2 His-55 with $OspC_A$ Glu-63 (**Figure 5C**). In terms of the B11 V_L domain, H-bonds occurred between LCDR1 Asn-31 and $OspC_A$ Lys-196, and LCDR1 Asn-32 with $OspC_A$ Glu-189. The B11 V_L domain formed a single salt bridge between LCDR2 Asp-50 with $OspC_A$ Lys-196 (**Figure 5D**).

Structural comparisons between B11 and B5 Fab-$OspC_A$ complexes.

As noted in the Introduction, we recently reported the structure of recombinant homodimeric $OspC_A$ complexed with the Fab fragments of the transmission blocking murine MAb, B5 [**PDB ID 7UIJ**] [26]. The B11 Fab-$OspC_A$ complex is reminiscent of that structure in that B5 and B11 Fabs engage with the lateral face of $OspC_A$ in a side-on orientation (**Figure 6A**). However, the B5 and B11 Fabs are offset relative to each other, with B5 membrane-distal and B11 membrane-proximal (**Figure 6A**). Moreover, while B5 Fabs are virtually perpendicular to $OspC_A$ (**Figure 6A**), B11 Fabs associate with $OspC_A$ at a slight angle, thereby positioning B11 Fabs closer to the spirochete outer surface (**Figure 6A**). Nevertheless, there is sufficient distance between B11's epitope on with $OspC_A$ and the spirochete membrane to accommodate an antibody as shown when we super positioned the HIV-1 IgG b12 (PDB ID: **1HZH**) onto the B11 Fab (**Figure 6B**). One possible orientation of OspC-B11 IgG relative to the bacterial outer surface is shown in **Figure S4**.

B5 IgG and B11 IgG also resemble each other in terms of OspC type specificity: they react with $OspC_A$, but not $OspC_B$ and $OspC_K$. To elucidate the structural basis of B11's specificity for $OspC_A$, we superpositioned $OspC_A$ from within the B11 Fab-$OspC_A$ complex onto the crystal structures of $OspC_B$ [**PDB ID 7UJ2**] and $OspC_K$ [**PDB ID 7UJ6**], which are structurally similar to $OspC_A$ (RMSDs 0.9 Å to 1.1 Å; **Figure S2**). Although the unliganded form of $OspC_A$ more closely resembles $OspC_K$ (RMSD of ~0.7 Å) than $OspC_B$ (RMSD of 1.0 Å), several structural features of $OspC_B$ and $OspC_K$ may account for the lack of B11 IgG recognition. The most notable is a Lys at position 113 in $OspC_B$ compared to a Gly at residue 114 in $OspC_A$. Lys-113 would be expected to sterically clash with B11 Ser-28 (**Figures S3A**, **S4A**). Furthermore, a "deletion" of Ala-74 within α-helix 1 of $OspC_B$ relative to $OspC_A$ alters the relative configuration of this region. The different conformation of this segment in $OspC_B$ would position residue Lys-74 within 4 Å of B11 residue Arg-77 creating an electrostatic clash between these two positively charged residues (**Figures S3B, S5A**). In the case of $OspC_K$, the most prominent structural feature damping B11 recognition involves the change of Lys-161 in $OspC_A$, which H-bonds to Ser-56 of B11, to Ile-162 in $OspC_K$ thus precluding this interaction (**Figures S3C, S5A**).

Understanding the molecular basis of OspC type-immunospecificity is a longstanding challenge with relevance to vaccine design [42, 43]. We previously speculated that B5 IgG reactivity is restricted to just three OspC types (A, C3 and I3), based the variability of key paratope-epitope contacts [38]. By the same token, multiple sequence alignment (MSA) of 23 prominent *B. burgdorferi* OspC types suggest that B11 is similarly restricted. The primary sequences of four of the 23 OspC Types (C3, I3, J, and M) examined contain the residues ostensibly associated with B11 recognition on Type A (**Figure S5B**). OspC types C3, I3, J, and M share 72-80% amino acid identity with $OspC_A$. More importantly, sequences within key B11-binding residues within each of these four OspC types are identical $OspC_A$. The main-chain structure around residue 74 is conserved (whereas a deletion exists in other types, as described above) and OspC types C3, I3, J, and M contain a glycine or nonbulky amino acid at position 114 alleviating potential steric clash with B11 that appears in other OspC types (as described above). Each of the four selected potential B11-binders possess a phenylalanine at position 177 which buries much of its bulky side chain in the interface with B11. The loss of this bulky side chain would diminish the interaction with B11 by ~22 $Å^2$ based on buried surface area

calculations with Phe-177 $Å^2$ as a serine residue as found in many of the 23 OspC genotypes. Finally, these four putative B11-binding OspC types also bear a lysine or arginine at residue 161, which putatively H-bonds with B11. From this information, we speculate that B11 likely recognizes four additional OspC types: C3, I3, J, and M (**Figure S5B**). This contrasts with B5 IgG, which we proposed is restricted to OspC types A, C3 and I3 [38]. Cross reactivity with I3 is not surprising given that is a naturally occurring chimera between $OspC_F$ and $OspC_A$ with the C-terminus (residues 128-199) derived from type A [44].

Discussion

OspC plays a pivotal role in *B. burgdorferi* tick-to-mammalian transmission and in early stages of dissemination. Although OspC may not be the sole determinant of spirochete dissemination, its importance is underscored by the fact that certain *ospC* genotypes are associated with more invasive *B. burgdorferi* clinical isolates [45-48]. From the host vantage point, *B. burgdorferi* infection is accompanied by a robust OspC-specific antibody response, which subjects the spirochetes to an enormous immune pressure that may contribute to bacterial clearance [42, 49]. Despite the centrality of OspC in both infection and immunity, a high-resolution molecular and structural picture OspC-antibody interactions is lacking in humans.

In this study, we solved the first structure of OspC complexed with Fabs from a human monoclonal antibody. The antibody, B11, was originally isolated by Blum and colleagues as a recombinant IgG1 with paired V_H and V_L sequences from single-cell sorted, blood-derived plasmablasts from a Lyme disease patient [9]. Recombinant B11 was shown to be bacteriostatic (without addition of human complement) and capable of promoting *B. burgdorferi* opsonophagocytosis in culture [9, 50]. We have extended those observations by confirming that B11 recognizes native OspC on the surface of *B. burgdorferi* strain B31 (but not strains expressing OspC type B or K) and has both complement-independent and -dependent activities against the spirochetes in culture. Based on these observations we predict that "B11-like" antibodies contribute to the reduction and/or clearance of an active *B. burgdorferi* infection in humans.

The crystal structure of B11 Fabs complexed with dimeric $OspC_A$ is remarkable in that it demonstrates antibody association with the lateral faces ("stem") of $OspC_A$, rather than the more surface exposed "dome". Considering that OspC is tethered to the spirochete outer membrane via

its lipidated N-terminus, the molecule is generally depicted as projecting perpendicularly from the spirochete surface [33-35]. In such an orientation, the predominantly variable residues face outwards, while conserved amino acids are membrane proximal [34, 35]. Thus, it is natural to assume that type-specific antibodies engage the dome region of OspC via their Fab elements in a top-down orientation [35]. That assumption was called into question by the structure of B5 Fab-$OspC_A$ [38], and further undermined by the structure of B11 Fab-$OspC_A$.

Perhaps it is worth turning things on their side when rethinking the nature of OspC-antibody interactions. Indeed, Lawson and colleagues pondered this exact possibility when scrutinizing the structures of OspC and related Vsps from *B. turicatae* [35]. They cite evidence to suggest that the N- and C-termini of OspC and Vsp1 dimers "…either adopt a mostly 'random coil' conformation or are disordered." If correct, they argue, then OspC is essentially bound to the spirochete by a flexible tail, thereby enabling the bulk of OspC to sit sideways or even "upside down" on the cell membrane. Moreover, they note that such an unconventional orientation would explain how IgM antibodies are able access the very C-terminal decapeptide of OspC, a linear epitope known as C10 [51]. In such a configuration, the Fc regions of antibodies like B11 IgG would protrude from the bacterial surface and be prime targets for components of the complement system and Fc receptors on phagocytes [50].

The structural elucidation of the of B11 Fab-OspC complex has implications when considering the design of OspC-based vaccine antigens. First, the B11 Fabs bridge the OspC-OspC' dimer interface. This observation indicates that B11 underwent affinity maturation in the context of dimeric (not monomeric) OspC. From the standpoint of vaccine design, preserving the dimeric interface of OspC antigens is paramount for eliciting potent B11- and B5-like antibodies, an observation that has been alluded to by others [52]. Second, a detailed view of B11 and B5's epitopes reveal the molecular basis of OspC type-specificity, a factor that has limited OspC's utility as a Lyme disease vaccine antigen [28, 42, 53]. However, considering the current exponential advances in protein modeling and design, the availability of structural B cell epitopes will prove invaluable. Finally, tt is worth noting that in separate efforts we have identified human monoclonal and camelid-derived single-domain antibodies that have pan-OspC reactivity (L. Cavacini, D. Vance, M. Rudolph, N. Mantis, *manuscripts in preparation*). High-resolution epitope mapping studies of those pan-reactive OspC antibodies are ongoing, alongside passive protection studies in mouse models of *B. burgdoferi* by tick-mediated infection.

Materials and Methods

Cloning and expression of B11 IgG

The B11 V_H and V_L coding regions were extracted from NCBI's BioProject database under accession PRJNA470931 (GSE114310) [9]. The B11 V_H and V_L coding regions were synthesized as gBlock™ dsDNA fragments (GenScript, Piscataway, NJ) and cloned in-frame into pcDNA3.1-based human IgG_1 Fc and kappa light chain expression plasmids, respectively [54, 55]. The two plasmids were co-transfected into Expi293 cells using ExpiFectamine293™ transfection reagents (Thermo Fisher Scientific, Waltham, MA), following manufacturer's instructions. Five to six days later, supernatants containing the secreted antibodies were harvested and clarified before being subjected to protein A chromatography. Affinity purified IgG_1 B11 was then subjected to buffer exchange into PBS and stored at 4 °C. B11 Fabs were generated as described [38]. Purification and specificity of MAbs B5 [38]and hPB10 [56]have been previously described.

Cloning, expression, and purification of OspC

Recombinant $OspC_A$ (residues 38 to 201) from *B. burgdorferi* B31 [UniProt: accession Q07337] was expressed and purified as a homodimer from *E. coli*, as described [38].

B. burgdorferi strains and culture conditions

B. burgdorferi strains expressing OspC types A (B313), B (ZS7), K (297), and the *ospC* deletion strain B31A3ΔospC were cultured in BSK-II medium at 37°C with 5% CO_2 to mid-log phase [57], collected by centrifugation (3,300 × *g*), washed, suspended in BSK II with 20% glycerol and stored at -20 ºC until needed. Strains B313 [40], ZS7, and B31A3Δ*ospC* ("*ospC*K1") were kindly provided by Dr. Yi-Pin Lin (Wadsworth Center). Strain 297 was obtained from the American Type Culture Collection (ATCC; Manasas,VA).

A strain of *B. burgdorferi* B31 was engineered to deliver consistent ectopic expression of *ospC* under *in vitro* culturing conditions (BSK-II at 37°C). An IPTG-inducible *rpoS* expression plasmid was created through modification of the pBSV2G-derived *mCherry* plasmid, pGW163 [58]. Briefly, the *rpoS* open reading frame (ORF) was amplified from *B. burgdorferi* B31 [NCBI:txid224326] genomic DNA using Q5 DNA polymerase (NEB, Beverly, MA) and the

b31_rpoS_gibson_F (5'- agaattcattaaagaggagaaattacccatgaacatatttagtaatgaggatttaaacat -3') and b31_rpoS_gibson_R (5'-gtaaaacgacggccagtgccaagcttaatttatttcttcttttaatttttaagaactc-3') tailed primer set. The *mCherry* ORF was excised from pGW163 using NcoI and HindIII (NEB) and subsequently replaced with the tailed *rpoS* DNA fragment using the HiFi DNA assembly kit (NEB). Following the assembly reaction, the DNA was transformed into NEB® 5-alpha F' I q chemically competent cells (NEB). Recombinants were selected on LB agar supplemented with 10 µg/ml of gentamicin. Transformants that arose following overnight incubation at 30°C were screened via PCR using the b31_rpoS_gibson_F and b31_rpoS_gibson_R primer set. The IPTG-inducible *rpoS* expression plasmid, pGW181, was isolated from a single PCR-positive colony. Following purification from a large batch culture, pGW181 was electrotransformed into *B. burgdorferi* B31 as described [59], ultimately yielding the IPTG-inducible *rpoS* expression strain, GGW941.

For routine culture, frozen aliquots of *B. burgdorferi* were thawed and used to inoculate modified BSK-II lacking gelatin, supplemented with 6% rabbit serum (Pel-Freeze Biologicals, Rogers, AR) [60]. Base BSK-II medium was prepared by the Wadsworth Center's Tissue and Media Core Facility and filter sterilized (0.2 µm) prior to use. Cultures were maintained at 37°C with 5% CO_2 and passaged by dilution (1:10,000) into fresh BSK-II medium. *B. burgdorferi* cultures were routinely inspected for culture viability and motility during *in vitro* culture maintenance prior to the initiation of any experiments.

To induce RpoS expression, GGW941 culture medium was spiked with 250 µM IPTG at 24 h before use. For flow cytometry and microscopy studies (as described below), *B. burgdorferi* cells were collected in mid-logarithmic phase (~1-3 × 10^7 spirochetes per mL). As controls, spirochetes were heat killed by incubation at 56°C for at least 30 min, as described [61].

B. burgdorferi **motility determinations by dark field microscopy**

Mid-log-phase cultures of GGW941 treated 24 h prior with IPTG to induce *rpoS* expression, were adjusted to 5 x 10^6 bacteria per 50 µL in PBS then treated with indicated OspC MAbs (1, 2, 3, 10, 20, 30 µg/mL) in the presence or absence of 20% human complement (Sigma-Aldrich) for 16 or 24 h. Cultures were examined in a double-blind fashion by dark-field microscopy for motile spirochetes. 1:5 dilutions of the reactions were prepared by aspirating from the center of the reaction and diluted into fresh BSK-II medium. Dark-field microscopy was performed

utilizing a Trinocular DF microscope (AmScope) equipped with a camera with reduction lens (AmScope SKU: MU1603) using a 40× dry darkfield condenser (AmScope; DK-DRY200). Spirochetes were considered dead when complete loss of motility and refractivity was observed. Spirochetes were enumerated in 4 visual fields, and the percent viability was calculated as the ratio of live spirochetes (mean of 4 fields) in treated samples to spirochetes in the untreated control samples (mean of 4 fields). Polyclonal serum from *B. burgdorferi*-infected mice and MAb B5 were used as positive controls; naive serum and the PB10 isotype were used as negative controls. This experimental set up was conducted over the course of three independent sessions and data is plotted as the means for the three days of counting. Statistical analysis was determined using 2-way ANOVA with Dunnett's multiple comparisons test in which experimental means (B11, B5) were compared to control mean (PB10) for each antibody concentration.

Flow Cytometry

To examine the ability of B11 and B5 IgG1 to bind the spirochete surface and promote bacterial agglutination, and membrane permeability, *B. burgdorferi* strains expressing OspC types A (B313), B (ZS7), and K (297), were cultured, treated with 10 µg/ml IgG1, and analyzed by flow cytometry as described [38]. Briefly, an Alexa Fluor 647-labeled goat anti-human IgG [H+L] secondary antibody (Invitrogen) was used to detect bound IgG1 to the bacterial surface, and propidium iodide staining was used to indicate bacterial membrane permeability. The *ospC* deletion strain B31-A3*ospC*K1was used as a negative strain control, and the ricin toxin MAb, PB10, was used as an IgG1 isotype control. Bacteria were analyzed on a BD FACSCalibur (BD Biosciences). Voltage was set with untreated bacteria as a reference point (gMFI~ 5.0), and bacteria were gated on forward scatter (FSC) and side scatter (SSC) to exclude debris and assess aggregate size and granularity. Agglutination was calculated as the sum of events in the upper-left, upper-right, and lower-right quadrants relative to the total event counted (20,000).

Epitope mapping of B11 by HX-MS

Stock concentrations of $OspC_A$ (8.5 µM) in PBS alone or in a complex with a 2-fold molar excess of antibody B11 were diluted into 90 µL of deuterated PBS buffer (20 mM phosphate, 150 mM NaCl, 0.02% sodium azide, 1 mM EDTA pH* 7.54, 85%D final) containing 0.2 nM

bradykinin and incubated 3 sec on ice, or either 3 seconds, 1 minute, 30 minutes, or 20 hours at 21°C. Each starting stock also included a mixture of imidazolium compounds to serve as exchange reference standards [62]. At the desired time point the sample was rapidly mixed with an equal volume of ice cold 0.2% formic acid and 0.1% trifluoroacetic acid (TFA) for a final pH of 2.5. Samples were then immediately frozen on ethanol/dry ice and stored at -80°C until LC-MS analysis. Undeuterated samples were prepared the same way but with undeuterated buffer for each step.

Samples were thawed at 5°C for 8 minutes and injected using a custom LEAP robot integrated with an LC-MS system [63]. The protein was first passed over a Nepenthesin II column (2.1 x 30 mm; AffiPro) at 400 µL/min for inline digestion with the protease column held at 20°C. Peptides were then trapped on a Waters XSelect CSH C18 trap cartridge column (2.1 x 5 mm 2.5 µm) and resolved over a CSH C18 column (1 x 50 mm 1.7 µm 130Å) using linear gradient of 5 to 35% B (A: 0.1% FA, 0.025% TFA, 5% ACN; B: ACN with 0.1% FA) over 10 minutes and analyzed on a Thermo Orbitrap Ascend mass spectrometer at a resolution setting of 120,000. A series of washes over the trap and pepsin columns was used between injections to minimize carry-over as described [63]. Data dependent MS/MS acquisition was performed on an undeuterated sample using rapid CID and HCD scans and processed in Byonic (Protein Metrics) with a score cutoff of 150 to identify peptides. Deuterium incorporation was analyzed using HDExaminer v3 (Sierra Analytics).

Crystallization and data collection.

Fab B11 was complexed with dimeric $OspC_A$ in a 1:1 stoichiometry, then concentrated to 10 mg/ml final for all crystallization trials. Crystals were grown by sitting drop vapor diffusion using a protein to reservoir volume ratio of 1:1 with total drop volumes of 0.2 µl. Crystals of the B11 Fab-$OspC_A$ complex were produced at 22°C using a crystallization solution containing 100 mM sodium HEPES [pH 6.5], 18.6% PEG 6K, and 6.6 mM prasseodymium acetate. All crystals were flash frozen in liquid nitrogen after a short soak in the appropriate crystallization buffers supplemented with 10% ethylene glycol. Data were collected at the 24-ID-E beamline at the Advanced Photon Source, Argonne National Labs. All data was indexed, merged, and scaled using HKL2000[64] then converted to structure factor amplitudes using CCP4 [65].

Structure determination and refinement.

The B11 Fab-$OspC_A$ complex structure was solved by molecular replacement using Phaser [64]. Molecular replacement calculations were performed using the V_L and C_L domain coordinates of the human monoclonal mAb MAB4-5 (PDB ID: 5Y11) along with the V_H and C_H1 domains from the human anti-HIV antibody (PDB ID: 5UBY) as the search model for the first two B11 Fabs in B11-$OspC_A$ complex within the asymmetric unit. The $OspC_A$ coordinates (PDB ID: 1GGQ) were then used as the search model for the $OspC_A$ dimer in the first $OspC_A$-B11 complex. The initial B11-$OspC_A$ complex detected was then used to find the additional three B11-$OspC_A$ complexes present in the asymmetric unit. The resulting phase information from molecular replacement was used for some manual model building of the B11-$OspC_A$ structure using the graphics program COOT [66] and structural refinement employing the PHENIX package [67]. Data collection and refinement statistics are listed in **Table S1**, as is the Protein Data Bank (http://www.rcsb.org/pdb/) code for the B11-$OspC_A$ structure PDB ID 9BIF. The PDF validation report is provided in Supplemental Information. Molecular graphics were prepared using PyMOL (Schrodinger, DeLano Scientific LLC, Palo Alto, CA).

Data availability

All results and data files associated with this article are included in the main text and supplemental material.

Supporting information

This article contains supporting information, including supplemental tables with X-ray crystallography conditions, supplemental figures related to epitope mapping, and HX-MS data files and PDB validation report.

Acknowledgements

We are grateful to Drs. Lisa Blum and William Robinson (Stanford University) for sharing the B11 VH and VL sequences and for follow-up discussions. We thank Dr. Renjie Song at the Wadsworth Center's Immunology Core facility for assistance with flow cytometry. We thank the DNA sequencing core and members of the Wadsworth Center's bioinformatics core for useful

discussions. As always, we are grateful to Elizabeth Cavosie (Wadsworth Center) and Donna DeLuca (Health Research, Inc) for administrative assistance and program overview.

Funding sources

This work was supported by the National Institute of Allergy and Infectious Diseases (NIAID), National Institutes of Health (NIH), Department of Health and Human Services Contract No. 75N93019C00040. X-ray analysis as conducted at the Northeastern Collaborative Access Team beamlines, which are funded by P30 GM124165 from the National Institute of General Medical Sciences (NIGMS), NIH. The Eiger 16M detector on the 24-ID-E beam line is funded by a NIH-ORIPHEI grant (S10OD021527). HDX-MS studies conducted at the University of Washington was supported by award S10OD030237 from NIGMS. The content is solely the responsibility of the authors and does not necessarily represent the official views of the NIH.

Conflict of interest

The authors have no conflicts of interest to declare.

References

[1] Kugeler KJ, Schwartz AM, Delorey MJ, Mead PS, Hinckley AF. Estimating the Frequency of Lyme Disease Diagnoses, United States, 2010-2018. Emerg Infect Dis. 2021;27:616-9.

[2] Bobe JR, Jutras BL, Horn EJ, Embers ME, Bailey A, Moritz RL, et al. Recent Progress in Lyme Disease and Remaining Challenges. Front Med (Lausanne). 2021;8:666554.

[3] Radolf JD, Strle K, Lemieux JE, Strle F. Lyme Disease in Humans. Curr Issues Mol Biol. 2021;42:333-84.

[4] Steere AC, Strle F, Wormser GP, Hu LT, Branda JA, Hovius JW, et al. Lyme borreliosis. Nat Rev Dis Primers. 2016;2:16090.

[5] Lochhead RB, Strle K, Arvikar SL, Weis JJ, Steere AC. Lyme arthritis: linking infection, inflammation and autoimmunity. Nat Rev Rheumatol. 2021;17:449-61.

[6] Klempner MS, Hu LT, Evans J, Schmid CH, Johnson GM, Trevino RP, et al. Two controlled trials of antibiotic treatment in patients with persistent symptoms and a history of Lyme disease. N Engl J Med. 2001;345:85-92.

512 [7] Marques A. Chronic Lyme disease: a review. Infect Dis Clin North Am. 2008;22:341-60, vii-
513 viii.
514 [8] Aucott JN, Yang T, Yoon I, Powell D, Geller SA, Rebman AW. Risk of post-treatment Lyme
515 disease in patients with ideally-treated early Lyme disease: A prospective cohort study. Int J
516 Infect Dis. 2022;116:230-7.
517 [9] Blum LK, Adamska JZ, Martin DS, Rebman AW, Elliott SE, Cao RRL, et al. Robust B Cell
518 Responses Predict Rapid Resolution of Lyme Disease. Front Immunol. 2018;9:1634.
519 [10] Rousselle JC, Callister SM, Schell RF, Lovrich SD, Jobe DA, Marks JA, et al. Borreliacidal
520 antibody production against outer surface protein C of Borrelia burgdorferi. J Infect Dis.
521 1998;178:733-41.
522 [11] Barbour AG, Jasinskas A, Kayala MA, Davies DH, Steere AC, Baldi P, et al. A genome-
523 wide proteome array reveals a limited set of immunogens in natural infections of humans and
524 white-footed mice with Borrelia burgdorferi. Infect Immun. 2008;76:3374-89.
525 [12] Cadavid D, Pennington PM, Kerentseva TA, Bergstrom S, Barbour AG. Immunologic and
526 genetic analyses of VmpA of a neurotropic strain of Borrelia turicatae. Infect Immun.
527 1997;65:3352-60.
528 [13] Hubner A, Yang X, Nolen DM, Popova TG, Cabello FC, Norgard MV. Expression of
529 Borrelia burgdorferi OspC and DbpA is controlled by a RpoN-RpoS regulatory pathway. Proc
530 Natl Acad Sci U S A. 2001;98:12724-9.
531 [14] Pal U, Yang X, Chen M, Bockenstedt LK, Anderson JF, Flavell RA, et al. OspC facilitates
532 Borrelia burgdorferi invasion of Ixodes scapularis salivary glands. J Clin Invest. 2004;113:220-
533 30.
534 [15] Tilly K, Krum JG, Bestor A, Jewett MW, Grimm D, Bueschel D, et al. Borrelia burgdorferi
535 OspC protein required exclusively in a crucial early stage of mammalian infection. Infect
536 Immun. 2006;74:3554-64.
537 [16] Tilly K, Bestor A, Jewett MW, Rosa P. Rapid clearance of Lyme disease spirochetes
538 lacking OspC from skin. Infect Immun. 2007;75:1517-9.
539 [17] Earnhart CG, Leblanc DV, Alix KE, Desrosiers DC, Radolf JD, Marconi RT. Identification
540 of residues within ligand-binding domain 1 (LBD1) of the Borrelia burgdorferi OspC protein
541 required for function in the mammalian environment. Mol Microbiol. 2010;76:393-408.

[18] Caine JA, Coburn J. Multifunctional and Redundant Roles of Borrelia burgdorferi Outer Surface Proteins in Tissue Adhesion, Colonization, and Complement Evasion. Front Immunol. 2016;7:442.

[19] Lin YP, Tan X, Caine JA, Castellanos M, Chaconas G, Coburn J, et al. Strain-specific joint invasion and colonization by Lyme disease spirochetes is promoted by outer surface protein C. PLoS Pathog. 2020;16:e1008516.

[20] Tan X, Castellanos M, Chaconas G. Choreography of Lyme Disease Spirochete Adhesins To Promote Vascular Escape. Microbiol Spectr. 2023;11:e0125423.

[21] Zhong W, Gern L, Stehle T, Museteanu C, Kramer M, Wallich R, et al. Resolution of experimental and tick-borne Borrelia burgdorferi infection in mice by passive, but not active immunization using recombinant OspC. Eur J Immunol. 1999;29:946-57.

[22] Gilmore RD, Jr., Kappel KJ, Dolan MC, Burkot TR, Johnson BJ. Outer surface protein C (OspC), but not P39, is a protective immunogen against a tick-transmitted Borrelia burgdorferi challenge: evidence for a conformational protective epitope in OspC. Infect Immun. 1996;64:2234-9.

[23] Mbow ML, Gilmore RD, Jr., Titus RG. An OspC-specific monoclonal antibody passively protects mice from tick-transmitted infection by Borrelia burgdorferi B31. Infect Immun. 1999;67:5470-2.

[24] Gilmore RD, Jr., Piesman J. Inhibition of Borrelia burgdorferi migration from the midgut to the salivary glands following feeding by ticks on OspC-immunized mice. Infect Immun. 2000;68:411-4.

[25] Earnhart CG, Buckles EL, Dumler JS, Marconi RT. Demonstration of OspC type diversity in invasive human lyme disease isolates and identification of previously uncharacterized epitopes that define the specificity of the OspC murine antibody response. Infect Immun. 2005;73:7869-77.

[26] Wang IN, Dykhuizen DE, Qiu W, Dunn JJ, Bosler EM, Luft BJ. Genetic diversity of ospC in a local population of Borrelia burgdorferi sensu stricto. Genetics. 1999;151:15-30.

[27] Barbour AG, Travinsky B. Evolution and distribution of the ospC Gene, a transferable serotype determinant of Borrelia burgdorferi. MBio. 2010;1.

571 [28] Di L, Akther S, Bezrucenkovas E, Ivanova L, Sulkow B, Wu B, et al. Maximum antigen
572 diversification in a lyme bacterial population and evolutionary strategies to overcome pathogen
573 diversity. ISME J. 2022;16:447-64.
574 [29] Bockenstedt LK, Hodzic E, Feng S, Bourrel KW, de Silva A, Montgomery RR, et al.
575 Borrelia burgdorferi strain-specific Osp C-mediated immunity in mice. Infect Immun.
576 1997;65:4661-7.
577 [30] Bhatia B, Hillman C, Carracoi V, Cheff BN, Tilly K, Rosa PA. Infection history of the
578 blood-meal host dictates pathogenic potential of the Lyme disease spirochete within the feeding
579 tick vector. PLoS Pathog. 2018;14:e1006959.
580 [31] Wilske B, Preac-Mursic V, Jauris S, Hofmann A, Pradel I, Soutschek E, et al.
581 Immunological and molecular polymorphisms of OspC, an immunodominant major outer surface
582 protein of Borrelia burgdorferi. Infect Immun. 1993;61:2182-91.
583 [32] Theisen M, Borre M, Mathiesen MJ, Mikkelsen B, Lebech AM, Hansen K. Evolution of the
584 Borrelia burgdorferi outer surface protein OspC. J Bacteriol. 1995;177:3036-44.
585 [33] Eicken C, Sharma V, Klabunde T, Owens RT, Pikas DS, Hook M, et al. Crystal structure of
586 Lyme disease antigen outer surface protein C from Borrelia burgdorferi. J Biol Chem.
587 2001;276:10010-5.
588 [34] Kumaran D, Eswaramoorthy S, Luft BJ, Koide S, Dunn JJ, Lawson CL, et al. Crystal
589 structure of outer surface protein C (OspC) from the Lyme disease spirochete, Borrelia
590 burgdorferi. EMBO J. 2001;20:971-8.
591 [35] Lawson CL, Yung BH, Barbour AG, Zuckert WR. Crystal structure of neurotropism-
592 associated variable surface protein 1 (Vsp1) of Borrelia turicatae. J Bacteriol. 2006;188:4522-30.
593 [36] Rudolph MJ, Davis SA, Haque HME, Ejemel M, Cavacini LA, Vance DJ, et al. Structure of
594 a transmission blocking antibody in complex with Outer surface protein A from the Lyme
595 disease spirochete, Borreliella burgdorferi. Proteins. 2023.
596 [37] Mbow ML, Gilmore RD, Jr., Stevenson B, Golde WT, Piesman J, Johnson BJ. Borrelia
597 burgdorferi-specific monoclonal antibodies derived from mice primed with Lyme disease
598 spirochete-infected Ixodes scapularis ticks. Hybrid Hybridomics. 2002;21:179-82.
599 [38] Rudolph MJ, Davis SA, Haque HME, Weis DD, Vance DJ, Piazza CL, et al. Structural
600 Elucidation of a Protective B Cell Epitope on Outer Surface Protein C (OspC) of the Lyme
601 Disease Spirochete, Borreliella burgdorferi. mBio. 2023;14:e0298122.

602 [39] Manso T, Folch G, Giudicelli V, Jabado-Michaloud J, Kushwaha A, Nguefack Ngoune V, et
603 al. IMGT(R) databases, related tools and web resources through three main axes of research and
604 development. Nucleic Acids Res. 2022;50:D1262-D72.
605 [40] Sadziene A, Wilske B, Ferdows MS, Barbour AG. The cryptic ospC gene of Borrelia
606 burgdorferi B31 is located on a circular plasmid. Infect Immun. 1993;61:2192-5.
607 [41] Frye AM, Ejemel M, Cavacini L, Wang Y, Rudolph MJ, Song R, et al. Agglutination of
608 Borreliella burgdorferi by Transmission-Blocking OspA Monoclonal Antibodies and
609 Monovalent Fab Fragments. Infect Immun. 2022:e0030622.
610 [42] Baum E, Randall AZ, Zeller M, Barbour AG. Inferring epitopes of a polymorphic antigen
611 amidst broadly cross-reactive antibodies using protein microarrays: a study of OspC proteins of
612 Borrelia burgdorferi. PLoS One. 2013;8:e67445.
613 [43] O'Bier NS, Hatke AL, Camire AC, Marconi RT. Human and Veterinary Vaccines for Lyme
614 Disease. Curr Issues Mol Biol. 2021;42:191-222.
615 [44] Girard YA, Travinsky B, Schotthoefer A, Fedorova N, Eisen RJ, Eisen L, et al. Population
616 structure of the lyme borreliosis spirochete Borrelia burgdorferi in the western black-legged tick
617 (Ixodes pacificus) in Northern California. Appl Environ Microbiol. 2009;75:7243-52.
618 [45] Seinost G, Dykhuizen DE, Dattwyler RJ, Golde WT, Dunn JJ, Wang IN, et al. Four clones
619 of Borrelia burgdorferi sensu stricto cause invasive infection in humans. Infect Immun.
620 1999;67:3518-24.
621 [46] Hanincova K, Mukherjee P, Ogden NH, Margos G, Wormser GP, Reed KD, et al.
622 Multilocus sequence typing of Borrelia burgdorferi suggests existence of lineages with
623 differential pathogenic properties in humans. PLoS One. 2013;8:e73066.
624 [47] Lemieux JE, Huang W, Hill N, Cerar T, Freimark L, Hernandez S, et al. Whole genome
625 sequencing of human Borrelia burgdorferi isolates reveals linked blocks of accessory genome
626 elements located on plasmids and associated with human dissemination. PLoS Pathog.
627 2023;19:e1011243.
628 [48] Mukherjee PG, Liveris D, Hanincova K, Iyer R, Wormser GP, Huang W, et al. Borrelia
629 burgdorferi Outer Surface Protein C Is Not the Sole Determinant of Dissemination in Mammals.
630 Infect Immun. 2023;91:e0045622.

631 [49] Liang FT, Yan J, Mbow ML, Sviat SL, Gilmore RD, Mamula M, et al. Borrelia burgdorferi
632 changes its surface antigenic expression in response to host immune responses. Infect Immun.
633 2004;72:5759-67.
634 [50] Jahanbani S, Hansen PS, Blum LK, Bastounis EE, Ramadoss NS, Pandrala M, et al.
635 Increased macrophage phagocytic activity with TLR9 agonist conjugation of an anti- Borrelia
636 burgdorferi monoclonal antibody. Clin Immunol. 2023;246:109180.
637 [51] Mathiesen MJ, Hansen K, Axelsen N, Halkier-Sorensen L, Theisen M. Analysis of the
638 human antibody response to outer surface protein C (OspC) of Borrelia burgdorferi sensu stricto,
639 B. garinii, and B. afzelii. Med Microbiol Immunol. 1996;185:121-9.
640 [52] Edmondson DG, Prabhakaran S, Norris SJ, Ullmann AJ, Piesman J, Dolan M, et al.
641 Enhanced Protective Immunogenicity of Homodimeric Borrelia burgdorferi Outer Surface
642 Protein C. Clin Vaccine Immunol. 2017;24.
643 [53] Probert WS, Crawford M, Cadiz RB, LeFebvre RB. Immunization with outer surface
644 protein (Osp) A, but not OspC, provides cross-protection of mice challenged with North
645 American isolates of Borrelia burgdorferi. J Infect Dis. 1997;175:400-5.
646 [54] Wang Y, Kern A, Boatright NK, Schiller ZA, Sadowski A, Ejemel M, et al. Pre-exposure
647 Prophylaxis With OspA-Specific Human Monoclonal Antibodies Protects Mice Against Tick
648 Transmission of Lyme Disease Spirochetes. J Infect Dis. 2016;214:205-11.
649 [55] Haque HME, Ejemel M, Vance DJ, Willsey G, Rudolph MJ, Cavacini LA, et al. Human B
650 Cell Epitope Map of the Lyme Disease Vaccine Antigen, OspA. ACS Infect Dis. 2022.
651 [56] Roy CJ, Ehrbar DJ, Bohorova N, Bohorov O, Kim D, Pauly M, et al. Rescue of rhesus
652 macaques from the lethality of aerosolized ricin toxin. JCI Insight. 2019;4.
653 [57] Barbour AG. Isolation and cultivation of Lyme disease spirochetes. Yale J Biol Med.
654 1984;57:521-5.
655 [58] Vance DJ, Basir S, Piazza CL, Willsey GG, Haque HME, Tremblay JM, et al. Single-
656 domain antibodies reveal unique borrelicidal epitopes on the Lyme disease vaccine antigen, outer
657 surface protein A (OspA). Infect Immun. 2024;92:e0008424.
658 [59] Samuels DS. Electrotransformation of the spirochete Borrelia burgdorferi. Methods Mol
659 Biol. 1995;47:253-9.
660 [60] Pollack RJ, Telford SR, 3rd, Spielman A. Standardization of medium for culturing Lyme
661 disease spirochetes. J Clin Microbiol. 1993;31:1251-5.

[61] Sadziene A, Barbour AG. Experimental immunization against Lyme borreliosis with recombinant Osp proteins: an overview. Infection. 1996;24:195-202.

[62] Murphree TA, Vorauer C, Brzoska M, Guttman M. Imidazolium Compounds as Internal Exchange Reporters for Hydrogen/Deuterium Exchange by Mass Spectrometry. Analytical Chemistry. 2020;92:9830-7.

[63] Watson MJ, Harkewicz R, Hodge EA, Vorauer C, Palmer J, Lee KK, et al. Simple Platform for Automating Decoupled LC-MS Analysis of Hydrogen/Deuterium Exchange Samples. J Am Soc Mass Spectrom. 2021;32:597-600.

[64] Otwinowski Z, Minor W. Processing of x-ray diffraction data collected in oscillation mode. . Methods in Enzymology 1997;276:307-26.

[65] Winn MD, Ballard CC, Cowtan KD, Dodson EJ, Emsley P, Evans PR, et al. Overview of the CCP4 suite and current developments. Acta Crystallogr D Biol Crystallogr. 2011;67:235-42.

[66] Emsley P, Lohkamp B, Scott WG, Cowtan K. Features and development of Coot. Acta Crystallogr D Biol Crystallogr. 2010;66:486-501.

[67] Adams PD, Afonine PV, Bunkoczi G, Chen VB, Davis IW, Echols N, et al. PHENIX: a comprehensive Python-based system for macromolecular structure solution. Acta Crystallogr D Biol Crystallogr. 2010;66:213-21.

Figure Legends

Figure 1. Reactivity of B11 and B5 with $OspC_A$ on live spirochetes. Flow cytometric analysis of B11 and B5 MAb reactivity with *B. burgdorferi* strains expressing OspC types A (B313), B (ZS7), or K (297). A B. burgdorferi B31 OspC mutant (B31-A3Δ*ospC*) was included as a control. (**A**) Representative fluorescence histograms where an Alexa Fluor 647-labeled anti-human IgG secondary antibody was used to detect bacterial surface bound IgG. Panels show B11 (blue) or B5 (gray) compared to the isotype control (PB10, black). Events positive for 647 fluorescence fall to the right of the isotype control. The percent and geometric mean fluorescence intensity (gMFI) of positive events for bacteria incubated with B11 (blue) and B5 (gray) are indicated on each panel. (**B**) Corresponding FSC/SSC dot plots. Events that are increased in size (FSC) and granularity (SSC) represent multi-bacteria aggregates as the result of antibody-mediated agglutination of live spirochetes. The percentage of events that are agglutinated is indicated (black) and was calculated from the sum of events with increased FSC and SSC, (UL+UR+LR quadrants), relative to the total events counted (20,000). The percent of events positive for propidium iodide staining, indicating membrane permeability, is labeled, and highlighted in red.

Figure 2. Complement-dependent and -independent effects of B5 and B11. Mid-log-phase cultures of *B. burgdorferi* strain GGW941 treated for 24 h with IPTG induce *rpoS* expression, were adjusted to 5 x 10^6 bacteria per 50 µL in BSK II without (left columns) and with (right columns) 20% human complement. Cultures were then treated with (**A**) B11, (**B**) B5 or (**C**) PB10 at indicated concentrations (x-axis). Sixteen hours later, the cultures were examined in a double-blind fashion by dark-field microscopy for motile spirochetes. Spirochetes were enumerated in 4 visual fields, and the percent viability was calculated as the ratio of live spirochetes (mean of 4 fields) in treated samples to spirochetes in the untreated control samples (mean of 4 fields). The experimental set up was conducted over the course of three independent sessions and data is plotted as the means for the three days of counting. Statistical analysis to determined significance (*, $p<0.05$) was done with 2-way ANOVA with Dunnett's multiple comparisons test for each B11 and B5 versus PB10 (isotype control) at each dose.

Figure 3. Localization of the B11 epitope on $OspC_A$ using HDX-MS. HDX changes upon the addition of (**A**) B11 IgG and B5 IgG are plotted on the structure of $OspC_A$ [PDB ID 1GGQ]. Regions with reduced deuterium exchange (more protected) are colored blue, while more deuterium exchange are colored red. (**B-G)** Deuterium uptake plots for unbound $OspC_A$ (black liunes), B5-$OspC_A$ (purple lines) and B11-$OspC_A$ (green lines) are shown for selected regions, with the panel letter corresponding to the labels in panel A. Error bars represent standard deviations from triplicate measurements. Comprehensive exchange data is provided as an Excel file as Supplemental material.

Figure 4. Structure of B11 Fab-$OspC_A$. (A) Side-on and (B) top-down ribbon diagrams of $OspC_A$ homodimer ($OspC_A$, $OspC_A$') in complex with B11 Fabs (B11, B11'). $OspC_A$ is colored in cyan and $OspC_A$' in green. The B11 Fab V_H and C_H1 elements are colored in salmon and V_L and C_L in light gray. The B11' Fab V_H and C_H1 elements are colored in magenta and V_L and C_L in yellow. The V_H and V_L domains (V_H,V_L) along with the N- and C-termini of $OspC_A$ and $OspC_A$' are labelled accordingly.

Figure 5. Detailed interactions between B11 and $OspC_A$ revealed from the co-crystal structure. (**A**) Ribbon structure (top-down view) of $OspC_A$ homodimer ($OspC_A$, cyan; $OspC_A$', green) in complex with a single B11 Fab (V_H and C_H1 elements, magenta; V_L and C_L, yellow). The $OspC_A$ residues that engage with B11 are colored blue. Key secondary structures (α-helices 1, 2, 3, 5, and 6) and all six CDRs are labeled; (**B**) Ribbon (left) and surface (right) depiction of an $OspC_A$ homodimer ($OspC_A$, cyan; $OspC_A$', green) with B11-interacting residues shaded in dark blue. $OspC_A$ N and C-termini are labelled N and C, respectively. Representations of key H-bonds (red dashes) and salt bridges (yellow dashes) between (**C**) $OspC_A$ (green) and B11' V_H domain (magenta) and (**D**) $OspC_A$ (green) and B11' V_L domain (yellow). Side chains are drawn as sticks and color coordinated to the main chain color, with nitrogen atoms shaded blue and oxygen atoms shaded red. CDR elements are labelled per convention: CDR-L1, -L3, -L3; CDR-H1, -H2, -H3. $OspC_A$ N and C-termini are labelled N and C, respectively. All drawings are depicted as ribbon diagrams except the molecular surface representation in panel B.

Figure 6. Structural comparison of B11-OspC$_A$ with and B5-OspC$_A$. (**A**) Superposition of B11-OspC$_A$ and B5-OspC$_A$ drawn as Cα-traces depicting the similar side-on approach of each Fab to OspC$_A$ while highlighting the greater distance of B5 from the N and C-termini of OspC$_A$ relative to the B11 position. OspC$_A$ is colored cyan and green while the B11 Fab V_H and C_H1 elements are colored in salmon red and V_L and C_L in light gray. The B11' Fab V_H and C_H1 elements are colored in magenta and V_L and C_L in yellow. B5 Fabs are colored dark gray. (**B**) Superposition of the anti-HIV IgG1 mAb (PDB ID 1HZH) drawn as a gray Ca-trace onto B11 also depicted as a Ca-trace revealed no significant steric clash between the OspCA-bound IgG and the spirochete membrane. The OspCA-B11 structure is colored identically to panel A in this figure.

Table 1. Functional activity associated with MAbs B11 and B5

		B11				B5			
Strain	**type**	**Binding (%)[a]**	**Binding (gMFI)[a]**	**Agg (%)[b]**	**PI + (%)[c]**	**Binding (%)[a]**	**Binding (gMFI)[a]**	**Agg (%)[b]**	**PI + (%)[c]**
Δ*ospC*	-	-0.1 +/- 0.1	-13.8 +/- 10.5	0.1+/- 0.1	0.0 +/- 0.2	5.5 +/- 12.3	55.3 +/- 128.8	0.1 +/- 0.2	0.2 +/- 0.7
B313	A	92.8 +/- 2.0	3822.3 +/- 1516.1	22.5 +/- 8.6	9.3 +/- 5.3	94.5 +/- 2.7	6903 +/- 1023	33.4 +/- 6.1	15.2 +/- 10.4
ZS7	B	0.3 +/- 0.4	-7.7 +/- 16.3	-0.1 +/- 0.1	-0.1 +/- 0.2	0.0 +/- 0.1	-3.7 +/- 18.1	-0.1 +/- 0.1	-0.1 +/- 0.2
297	K	1.5 +/- 3.5	0.9 +/- 13.0	-0.2 +/- 0.3	0.01+/- 0.3	-0.2 +/- 0.2	3.6 +/- 11.1	-0.1 +/- 0.2	0.0 +/- 0.1

[a], *B. burgdorferi* surface binding; [b], Agglutination; [c], propidium iodide positive events. Flow cytometric analysis of OspC IgG mAbs B11 and B5 and their reactivity with live *B. burgdorferi* strains expressing different OspC types. An anti-human IgG Alexa 647-labeled secondary antibody was used to detect mAb binding and is displayed as percentage of events positive for 647 fluorescence, and geometric mean fluorescence intensity (gMFI). The percentage of events with increased size and granularity (FSC/SSC) demonstrating agglutination, and percentage of events with propidium iodide uptake are shown. Displayed are mean values, with background subtraction, +/- standard deviation, n=4.

759
760

Table 2. Summary of B11-OspC$_A$ binding data and interface information

Interface(s)[a]	H-bonds [b]	SB [c]	SC [d]	Total BSA (Å^2)
1 (2)	4 (9)	3 (3)	0.51 (0.44)	2706 (2772)
3 (4)	12 (13)	2(3)	0.48 (53)	2671 (2710)
5 (6)	3 (8)	3(4)	0.59 (0.47)	2636 (2814)
7 (8)	8 (11)	3(3)	0.51 (0.59)	2406 (2600)

[a], primary and secondary (in parentheses) interfaces; [b],hydrogen bonds; [c], salt bridges; [d], shape complementarity score

761
762
763
764
765

Figure 1

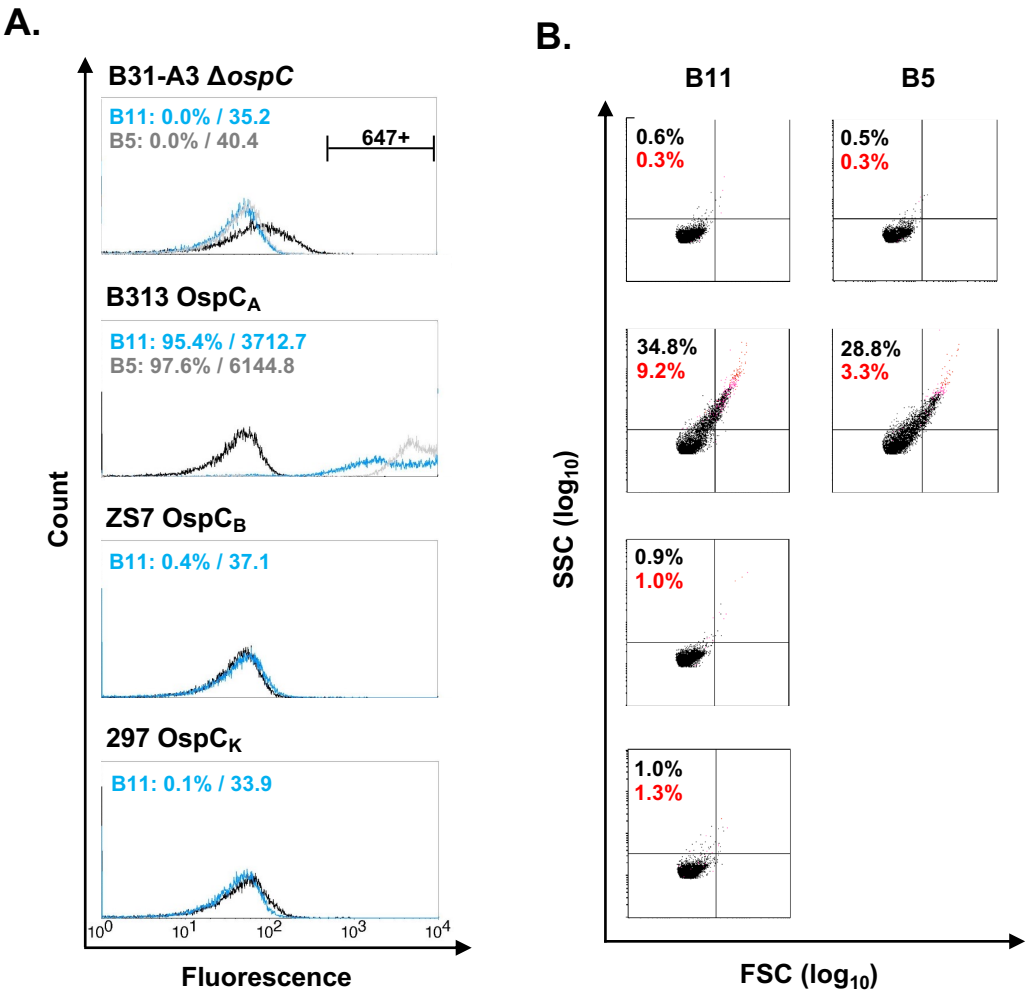
A.
B31-A3 ΔospC
B11: 0.0% / 35.2
B5: 0.0% / 40.4
647+
B313 OspC$_A$
B11: 95.4% / 3712.7
B5: 97.6% / 6144.8
ZS7 OspC$_B$
B11: 0.4% / 37.1
297 OspC$_K$
B11: 0.1% / 33.9
Count
10^0 10^1 10^2 10^3 10^4
Fluorescence
B.
B11
B5
0.6%
0.3%
0.5%
0.3%
34.8%
9.2%
28.8%
3.3%
0.9%
1.0%
1.0%
1.3%
SSC (log$_{10}$)
FSC (log$_{10}$)

Figure 2

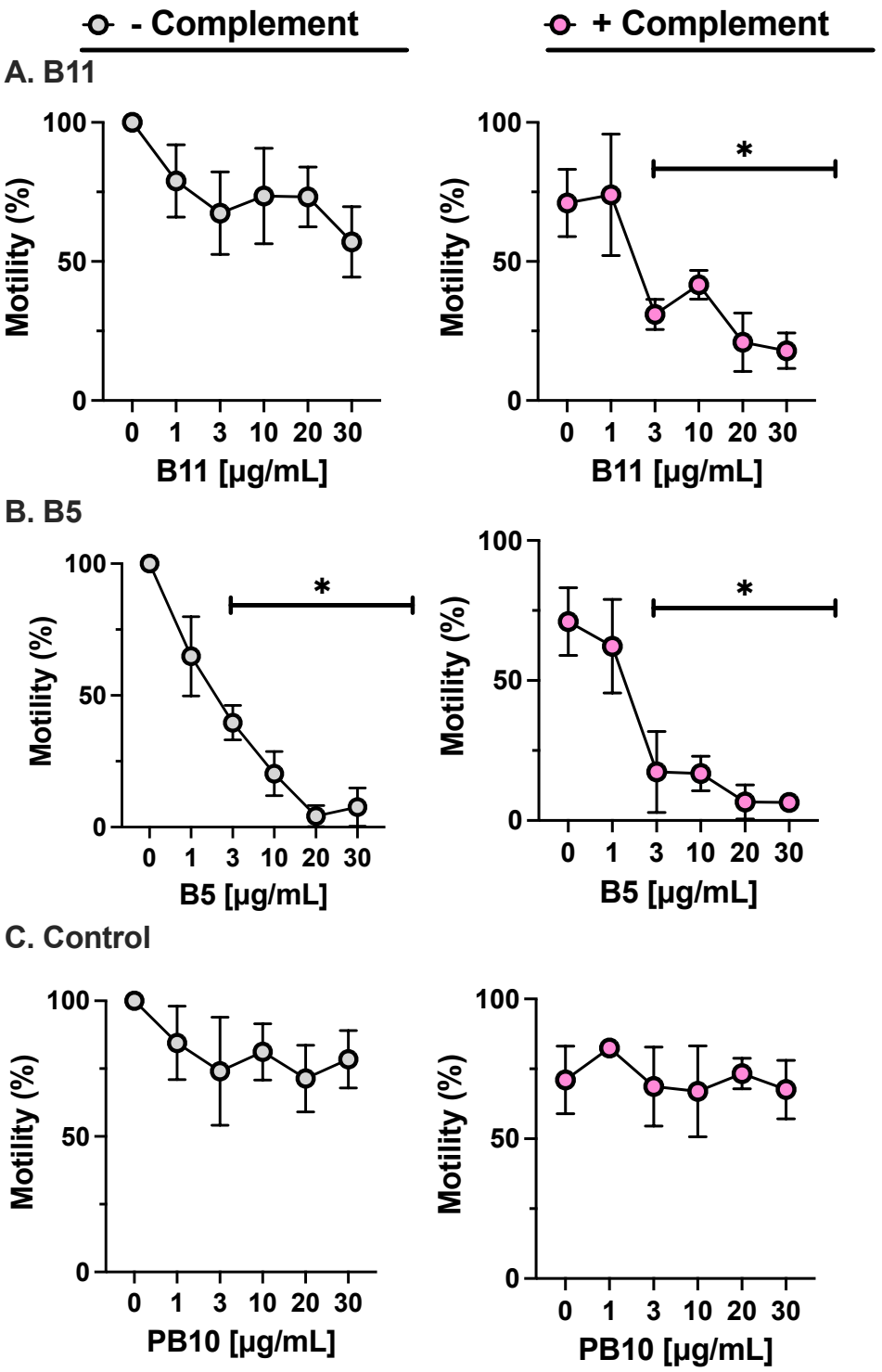
- Complement
+ Complement
A. B11
Motility (%)
100
50
0
0 1 3 10 20 30
B11 [µg/mL]
*
B. B5
B5 [µg/mL]
C. Control
PB10 [µg/mL]

Figure 3

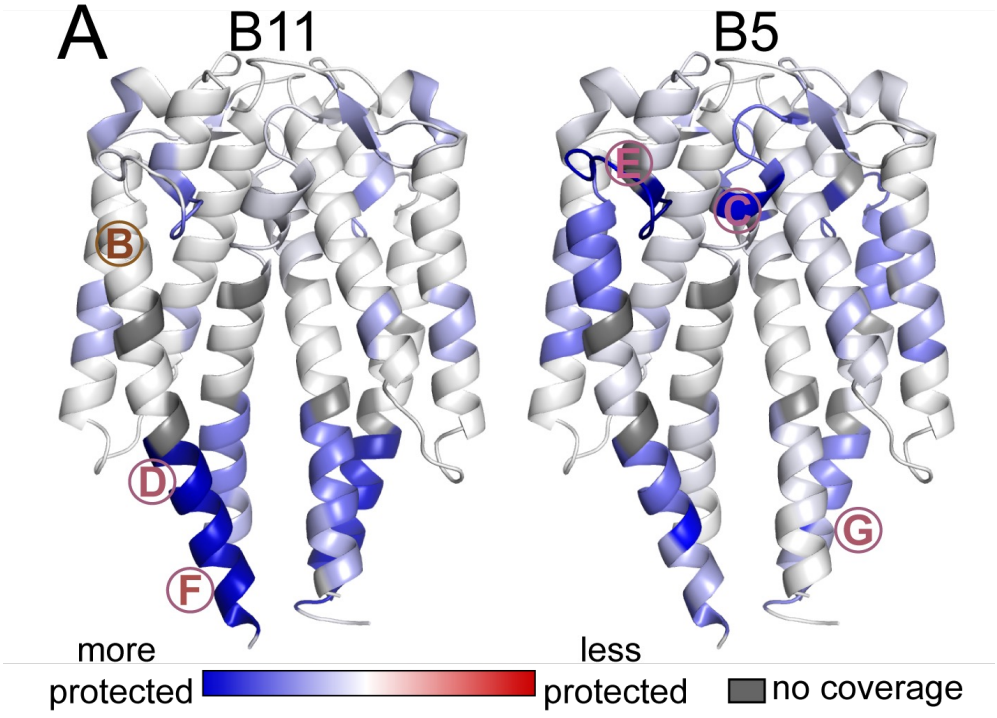
A
B11
B5
B
C
D
E
F
G
more protected
less protected
no coverage

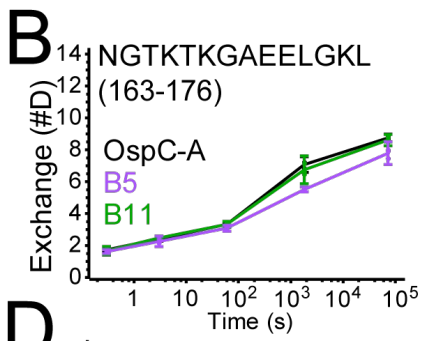
B
NGTKTKGAEELGKL
(163-176)
OspC-A
B5
B11
Exchange (#D)
Time (s)

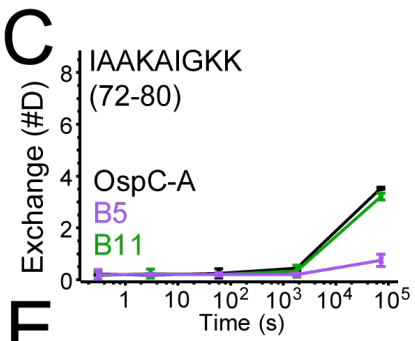
C
IAAKAIGKK
(72-80)
OspC-A
B5
B11
Exchange (#D)
Time (s)

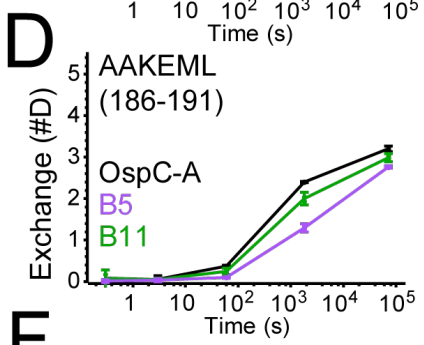
D
AAKEML
(186-191)
OspC-A
B5
B11
Exchange (#D)
Time (s)

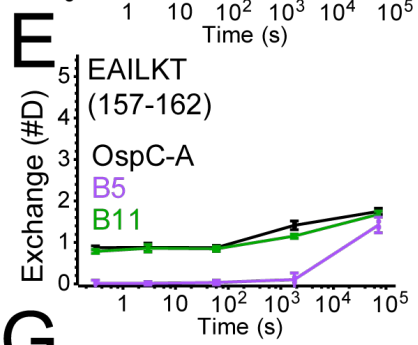
E
EAILKT
(157-162)
OspC-A
B5
B11
Exchange (#D)
Time (s)

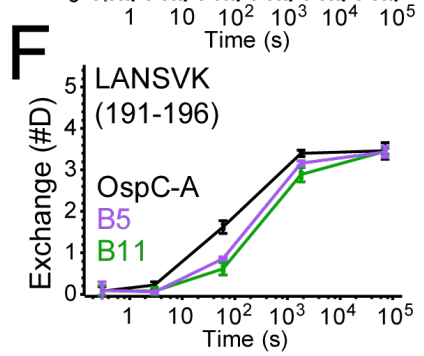
F
LANSVK
(191-196)
OspC-A
B5
B11
Exchange (#D)
Time (s)

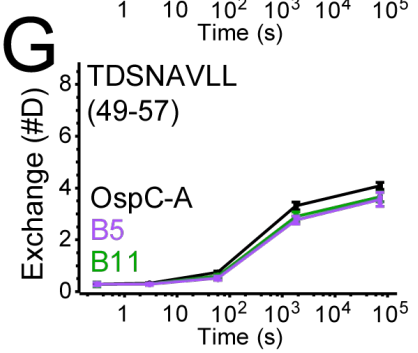
G
TDSNAVLL
(49-57)
OspC-A
B5
B11
Exchange (#D)
Time (s)

Figure 4

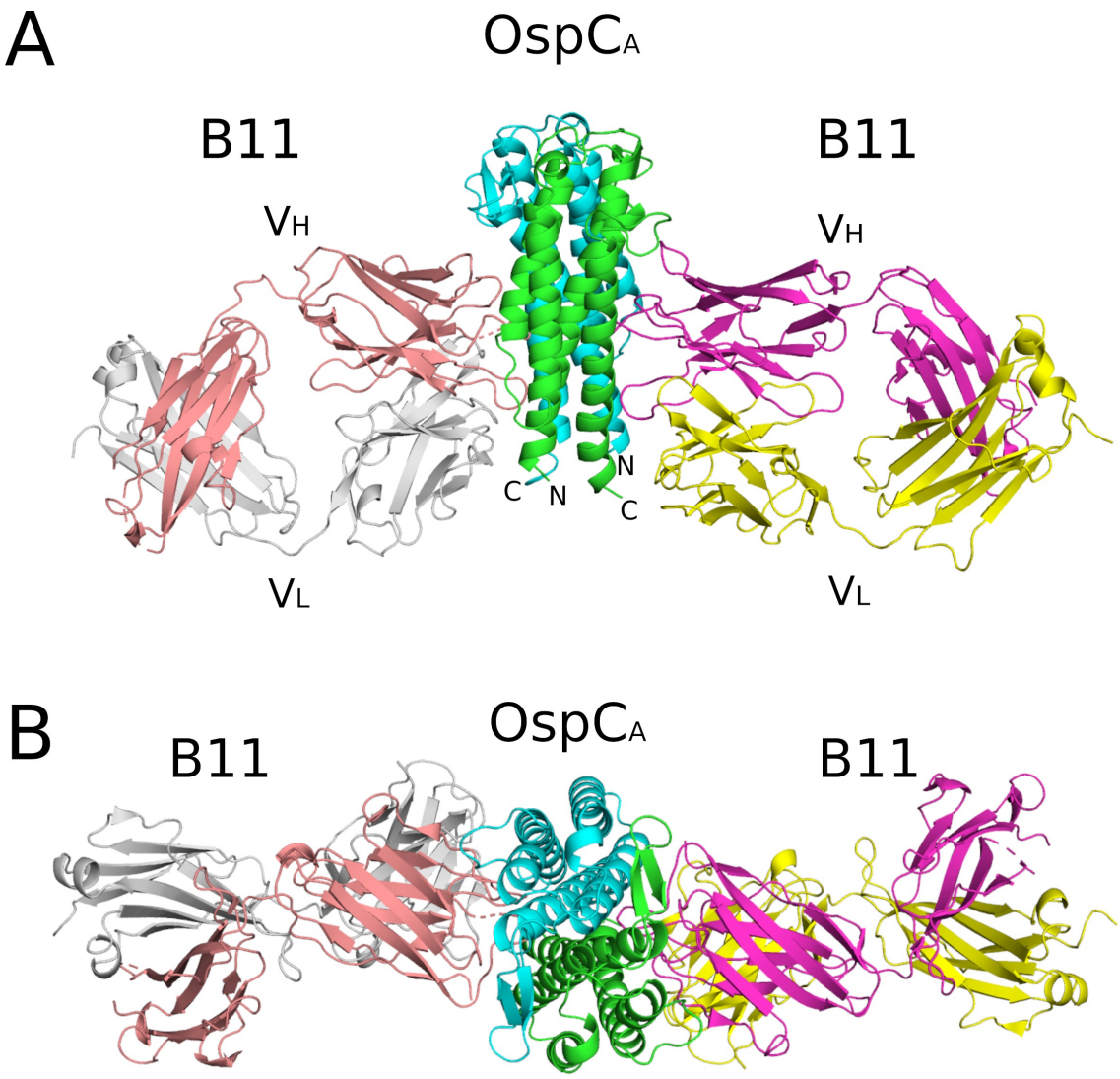

Figure 5

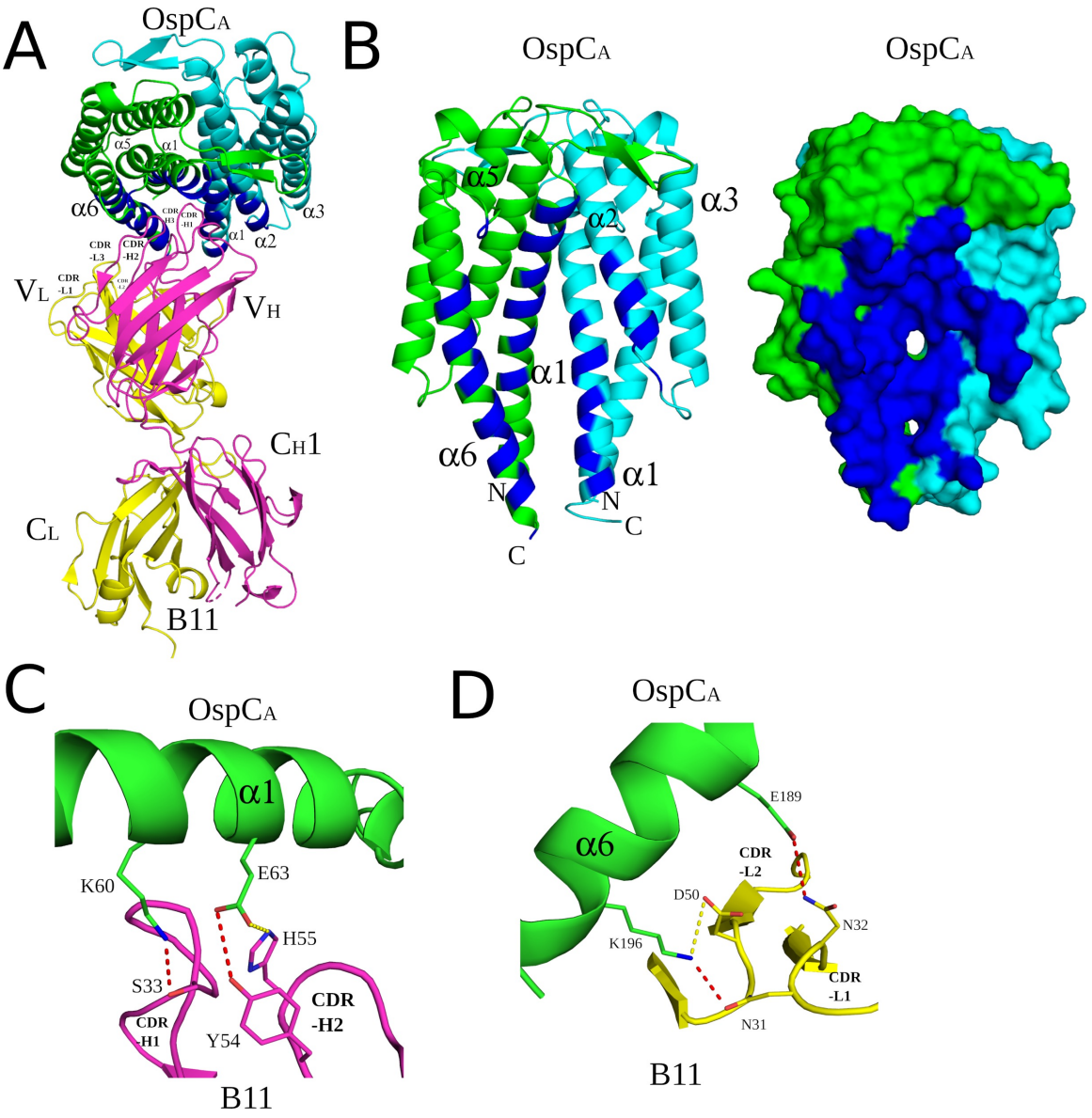
A
OspCA
α5
α1
α6
α3
α1
α2
CDR -L3
CDR -H2
CDR -L1
VL
VH
CH1
CL
B11
B
OspCA
α5
α2
α3
α1
α6
N
α1
N
C
C
OspCA
C
OspCA
α1
K60
E63
H55
S33
CDR -H1
Y54
CDR -H2
B11
D
OspCA
E189
α6
CDR -L2
D50
N32
K196
CDR -L1
N31
B11

Figure 6